Vehicle Yaw Stability Control by Coordinated Active Front Steering and Differential Braking in the Tire Sideslip Angles Domain

Stefano Di Cairano, *Member, IEEE*, Hongtei Eric Tseng, Daniele Bernardini, and Alberto Bemporad, *Fellow, IEEE*

***Abstract*— Vehicle active safety receives ever increasing attention in the attempt to achieve zero accidents on the road. In this paper, we investigate a control architecture that has the potential of improving yaw stability control by achieving faster convergence and reduced impact on the longitudinal dynamics. We consider a system where active front steering and differential braking are available and propose a model predictive control (MPC) strategy to coordinate the actuators. We formulate the vehicle dynamics with respect to the tire slip angles and use a piecewise affine (PWA) approximation of the tire force characteristics. The resulting PWA system is used as prediction model in a hybrid MPC strategy. After assessing the benefits of the proposed approach, we synthesize the controller by using a switched MPC strategy, where the tire conditions (linear/saturated) are assumed not to change during the prediction horizon. The assessment of the controller computational load and memory requirements indicates that it is capable of real-time execution in automotive-grade electronic control units. Experimental tests in different maneuvers executed on low-friction surfaces demonstrate the high performance of the controller.**

***Index Terms*— Automotive controls, hybrid control systems, model predictive control, vehicle stability control.**

I. Introduction

VEHICLE stability systems[1] are a major research area in automotive because of the demonstrated capabilities of reducing single-vehicle accidents [4], [5]. Recently the U.S. Government mandated the electronic stability control (ESC) to be mandatory in all new passenger cars in the United States, starting from 2012. ESC [6], [7] employs differential braking, i.e., different braking torques applied to different wheels, to generate a yaw moment that stabilizes the vehicle when this begins to drift. Differential braking has been proved very effective in stability recovery at the price of perturbing the longitudinal vehicle dynamics, and possibly causing undesired longitudinal decelerations.

Besides differential braking, other actuators can be used for stability control. Active steering allows the modification of the tire road wheel angle (RWA), i.e., the angle of the tire with respect to the vehicle longitudinal axis measured at the point of contact with the road. In particular, active front steering (AFS) systems [8] are capable of modifying the relation between the steering wheel angle (SWA), the command on the steering wheel, and the RWA at the front tires. Thus, AFS modifies the effective vehicle steering angle without changing the steering wheel position. Today, AFS is used in some passenger vehicles to improve cornering performance, but it has been investigated also for vehicle stabilization [8]. Although AFS has reduced authority with respect to differential braking, it is less intrusive for the driver, since it does not affect the longitudinal vehicle dynamics.

An even better solution that allows the retention of the strong stabilization capabilities of ESC and the fine regulation capabilities of AFS is to design a system that integrates both actuators [9], [10] for stabilizing the vehicle with minimal disturbance to the longitudinal dynamics. Such a system will be capable of improving both cornering performance and vehicle stabilization. However, coordinating AFS and ESC to achieve cornering performance and vehicle stabilization is challenging, and requires an appropriate control strategy. Several approaches have been investigated in recent years for vehicle stability control with different actuator configurations, including $\mathcal{H}_\infty$ control, μ-synthesis, dynamic control allocation, and sliding modes, see [8], [9], [11]–[14], and the references therein.

Model predictive control (MPC) [15] is a promising candidate for controlling systems with multiple constrained actuators. MPC exploits a model of the system dynamics to predict the future system evolution and to accordingly select the best control action with respect to a specified performance criterion. As opposed to standard optimal control, in MPC the input trajectory is recomputed every time new information on the system (e.g., a new state estimate) becomes available, hence implementing a feedback mechanism. At every control cycle, MPC computes the solution of a finite horizon optimal control problem formulated based on the system dynamics, performance criterion (cost function), and operating constraints. Thus, a particular advantage of MPC is the capability of coordinating several constrained actuators to

Manuscript received June 2, 2011; revised March 31, 2012; accepted April 11, 2012. Manuscript received in final form May 4, 2012. Date of publication June 13, 2012; date of current version June 14, 2013. Recommended by Associate Editor S. M. Savaresi.

S. Di Cairano was with Ford Research and Adv. Engineering, Dearborn, MI 48124 USA. He is now with Mitsubishi Electric Research Laboratories, Cambridge, MA 02139 USA (e-mail: dicairano@ieee.org).

H. E. Tseng is with the Powertrain Control R&A Department, Ford Research and Advanced Engineering, Dearborn, MI 48124 USA (e-mail: htseng@ford.com).

D. Bernardini and A. Bemporad are with the IMT Institute for Advanced Studies, Lucca 55100, Italy (e-mail: daniele.bernardini@imtlucca.it; alberto.bemporad@imtlucca.it).

Color versions of one or more of the figures in this paper are available online at http://ieeexplore.ieee.org.

Digital Object Identifier 10.1109/TCST.2012.2198886

[1]Preliminary studies related to this work were presented [1]–[3].

Fig. 1. RWD test vehicle equipped with AFS and differential braking used for experimental validation.

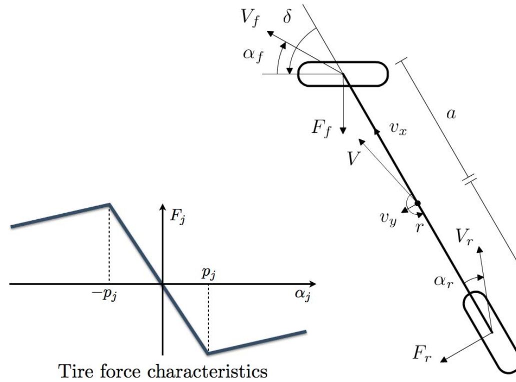

Fig. 2. (a) Qualitative approximation of the tire sideslip angle–tire force relation. (b) Schematics of the bicycle vehicle model.

achieve multiple goals encoded in the performance criterion. For several years, MPC has only been applied to systems with slow linear dynamics. However, the recent development of multiparametric programming [16], which allows the optimal control problem to be solved offline, and of MPC for hybrid systems [hybrid MPC (hMPC)] [17], [18] have considerably increased the domain of applicability. For instance, several applications have been proposed in automotive control, for engine [19]–[21], traction [22], actuators [23], and energy management [24], [25]. For vehicle stability control, linear-time varying MPC (LTV-MPC) and nonlinear MPC (NMPC) have been applied to autonomous vehicles in [26]. Dynamic control allocation [14] is also related to MPC.

In this paper, we consider the problem of stabilizing the vehicle dynamics and tracking the driver-requested yaw rate using differential braking and AFS. Differently from the autonomous vehicle context (e.g., [26]), here the controller has to interact with the driver, and it has very limited information on the desired trajectory and on the driver intent. In order to obtain an MPC controller that can execute at high rate on automotive-grade electronic control units (ECUs), we use MPC techniques for which the optimal solution is computed offline by multiparametric programming, thereby synthesizing the control law in the form of a (nonlinear) static state feedback. In Section II, by formulating the vehicle dynamics with respect to the tire sideslip angles and by considering a piecewise affine (PWA) approximation of the tire forces with respect to such angles, we obtain a PWA prediction model. In PWA systems [27], the state-input space is partitioned into polyhedral regions, and in each region an affine equation defines the system dynamics. Based on the PWA model, in Section III a hMPC strategy is developed to evaluate the system capabilities, and in particular the advantages of integrating AFS and differential braking with respect to using differential braking only. In order to reduce the computational complexity of the controller, in Section IV we propose an implementation based on a switched MPC (sMPC) strategy, where the system mode (the discrete state of the hybrid system) is assumed constant in prediction. The obtained controller is significantly simpler, resulting in a worst case computational load that allows for high-rate execution in automotive-grade computational platforms, and the stability properties of the closed-loop system can be assessed. In Section V we present experimental results in different maneuvers executed in the test vehicle shown in Fig. 1 on low friction surfaces (icy/packed/soft snow). Conclusions and future developments are summarized in Section VI.

Notation: $\mathbb{R}$, $\mathbb{R}_{0+}$, $\mathbb{Z}$, and $\mathbb{Z}_{0+}$ are the sets of real, nonnegative real, integer, nonnegative integer numbers, respectively. We indicate the identity by I, and a matrix of zeros by 0. For a matrix A, $[A]^m$ is the mth column, while for a vector v, $[v]_m$ is the mth component. Inequalities between vectors are intended componentwise, while for a matrix Q, $Q > 0$, ($Q \geq 0$) indicates positive (semi)definitiveness. With a little abuse of notation $\|x\|_Q^2 = x'Qx$.

We avoid to explicitly show the dependence from time when not needed. For discrete-time systems, $x(k)$ is the value of vector x at time kT_s and $a(h|k)$ the predicted value of $a(k+h)$ basing on data at time k.

II. Cornering Dynamics Model

In normal "on road" driving, which is the focus of this paper, the vehicle dynamics can be conveniently approximated by the bicycle model [28] shown on the right side of Fig. 2. Such model neglects vertical load transfer, which is important in performance driving [29], and track width, which is important at low speeds. Despite the reduced complexity, the bicycle model captures the relevant vehicle dynamics, and is appropriate for feedback control design [8], [9], [12], [26].

Since the focus of this paper is a driver-assist system where the controller does not have information about the road, we consider a reference frame that moves with the vehicle. The frame origin is at the vehicle center of mass, with the x-axis along the longitudinal vehicle direction pointing forward, the y-axis pointing to the left vehicle side, and the z-axis pointing upward. Here, we focus on the dynamics on the xy-plane, where, due to the choice of the reference frame, the angles increase counterclockwise. The tire sideslip angle (or simply slip angle) is the angle between the tire direction and the velocity vector at the tire. In the bicycle model, α_f[rad] and α_r[rad] are the tire sideslip angles at the front and at the rear tires, respectively. According to the chosen reference frame, the tire slip angles in Fig. 2 are negative.

By approximating the longitudinal velocity at the wheels as equal to the one at the center of mass, v_x [m/s], and the lateral

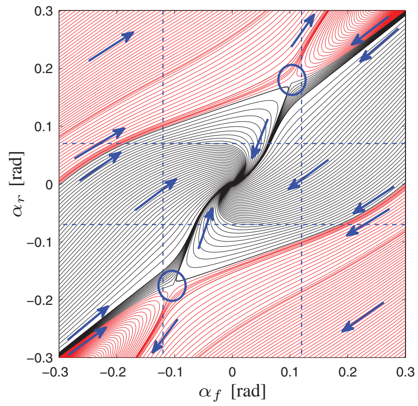

Fig. 3. Open-loop trajectories of the nonlinear vehicle dynamics in the tire slip angles domain for $\delta = 0$, $Y = 0$, and boundaries of the PWA regions.

velocity at the wheels as the sum of the lateral velocity at the center of mass v_y [m/s] and of the component due to rotation, we have

$$\tan(\alpha_f + \delta) = \frac{v_y + ar}{v_x}, \qquad \tan \alpha_r = \frac{v_y - br}{v_x} \tag{1}$$

where a[m] and b[m] are the distances of the front and rear wheel axels from the vehicle center of mass, respectively, δ [rad] is the steering angle at the road (RWA), and r [rad/s] is the yaw rate.

The front and rear tire forces F_f[N], F_r[N], respectively, are nonlinear functions of α_f, α_r, and of the longitudinal slip[2] $\sigma \in (0, 1)$. Based on a tire brush model (see [30]) for constant σ, which is a reasonable approximation for cornering in normal driving, we can approximate the tire forces as

$$F_j(\alpha_j) = \begin{cases} d_j(\alpha_j + p_j) - e_j, & \text{if} \quad \alpha_j < -p_j \\ c_j\alpha_j, & \text{if } -p_j \le \alpha_j \le p_j \\ d_j(\alpha_j - p_j) + e_j, & \text{if} \quad \alpha_j > p_j \end{cases} \tag{2}$$

where $j \in \{f, r\}$, $j = r$ for the rear tires, and $j = f$ for the front tires, p_j[rad] is called the *saturation angle*, and c_j[N/rad], d_j[N/rad], e_j[N] are identified from experimental data or from more complex tire models, e.g., [31]. Three regions of operations per pair of tires are considered, i.e., negative saturation ($\alpha_j < -p_j$), linear ($|\alpha_j| \le p_j$), and positive saturation ($\alpha_j > p_j$). A qualitative approximation of the sideslip angle–tire force characteristic is shown on the left side of Fig. 2, where it is shown that we allow for nonzero slope of the curve in the saturation regions. The tire forces (2) are symmetric, i.e., for any $\alpha_j \in \mathbb{R}$, $j \in \{f, r\}$, $F_j(-\alpha_j) = -F_j(\alpha_j)$.

In high-speed turns, the tire slip angles are small [28], hence (1) is suitably approximated by

$$\alpha_f = \frac{v_y + ar}{v_x} - \delta, \qquad \alpha_r = \frac{v_y - br}{v_x}. \tag{3}$$

By assuming a constant longitudinal velocity v_x and differentiating (3) we obtain

$$\dot{\alpha}_f = \frac{\dot{v}_y + a\dot{r}}{v_x} - \varphi, \qquad \dot{\alpha}_r = \frac{\dot{v}_y - b\dot{r}}{v_x} \tag{4}$$

[2]The normalized difference between driven and driving wheels velocities.

where $\varphi = \dot{\delta}$ [rad/s] is the steering angle rate. From (3)

$$\alpha_f - \alpha_r = \frac{v_y + ar}{v_x} - \delta - \frac{v_y - br}{v_x}$$

hence

$$r = \frac{v_x}{a + b}(\alpha_f - \alpha_r + \delta). \tag{5}$$

From (3) and (5), at steady state, α_f, α_r have opposite signs with respect to r, and in general $|\alpha_f| > |\alpha_r|$. Thus, at steady state, $r < (v_x)/(a + b\delta)$, according to the understeering behavior of passenger vehicles [28].

Under the indicated assumptions, the lateral acceleration can be decomposed into the acceleration of a frame rotating with yaw rate r, and the lateral acceleration at the center of mass

$$\dot{v}_y = \frac{F_f \cos\delta + F_r}{m} - rv_x. \tag{6}$$

The yaw acceleration is

$$\dot{r} = \frac{aF_f \cos\delta - bF_r + Y}{I_z} \tag{7}$$

where I_z[kgm^2] is the vehicle inertia along the z-axis, and Y[Nm] is the yaw moment obtained by differential braking, i.e., by applying different torques at different wheels. In (7), the four wheels braking torques are abstracted by the resulting yaw moment along the vehicle vertical axis, thereby reducing the model complexity.

The trajectories generated by (2), (6), and (7) for different initial values of α_f, α_r, and for $v_x = 15$ m/s, $\delta = 0$ rad, $Y = 0$ Nm are shown in the tire slip angles phase plane in Fig. 3, where also the saturation angle values are shown. The unstable trajectories are plotted in red and the stable trajectories in black. Beside the stable equilibrium at the origin, two unstable equilibria (circled) appears at approximately $(\alpha_f, \alpha_r) = \pm(0.095, 0.15)$. The location of the equilibria depends on the tire force characteristics (2) and on the steering angle, consistently with the analysis in [12], based on body slip angle and yaw rate.

For small steering angles, $\cos\delta \simeq 1$, hence substituting (5), (6), and (7) into (4) gives

$$\dot{\alpha}_f = \frac{F_f + F_r}{mv_x} - \frac{v_x}{a+b}(\alpha_f - \alpha_r + \delta) + \frac{a}{v_x I_z}(aF_f - bF_r + Y) - \varphi \tag{8a}$$

$$\dot{\alpha}_r = \frac{F_f + F_r}{mv_x} - \frac{v_x}{a+b}(\alpha_f - \alpha_r + \delta) - \frac{b}{v_x I_z}(aF_f - bF_r + Y) \tag{8b}$$

$$\dot{\delta} = \varphi. \tag{8c}$$

System (8) has state vector $x = [\alpha_f \ \alpha_r \ \delta]'$, input vector $u = [\varphi \ Y]'$, and output $y = r$, by (5). The dynamics (2), (5), and (8) are represented by the PWA system

$$\dot{x}(t) = A_i^c x(t) + B_i^c u(t) + \phi_i^c \tag{9a}$$

$$y(t) = C^c x(t) \tag{9b}$$

$$i(t) \in \mathcal{I} \ : \ H_{i(t)}x(t) \le K_{i(t)} \tag{9c}$$

where $x \in \mathbb{R}^3$, $u \in \mathbb{R}^2$, $y \in \mathbb{R}$, $i \in \mathcal{I}$ is the active region, $\mathcal{I} = \{1, \ldots, s\}$. Inequalities (9c) are obtained from the ranges of the linearizations in (2). The effect of (9c) is to partition the state space into polyhedral regions that define the operating conditions (linear, and positive and negative saturation, for front and rear tires), which are called the *modes* or the *regions* of the PWA system, in total, s. The matrices A_i, B_i, $i \in \mathcal{I}$ define the vehicle dynamics in the different conditions, and are obtained by substituting the linearized force equations (2) into (8). The active region i of the PWA system is selected by evaluating (9c) for the current value of the state x, i.e., the current value of tire sideslip angles and of the steering angle. There are three conditions for the front tires and three for the rear tires, hence $s = 9$, and the PWA vector field is symmetric with respect to the state-input vector.

Remark 1: Equation (9) is obtained for constant longitudinal velocity v_x and constant surface friction μ. In what follows, we show that the controller is robust to variations in vehicle velocity and friction. For improving model fidelity over a wider range of conditions, multiple models can be used.

III. Controller Design and Capabilities Evaluation by hMPC

The vehicle model developed in Section II is used for prediction in an MPC algorithm. The feedback nature of MPC is expected to compensate for the modeling approximations in Section II and aimed at reducing the complexity of the prediction model and of the control algorithm.

The controller designed here has to track the desired yaw rate while keeping the slip angles within acceptable bounds. At every control cycle, the general MPC algorithm performs the following operations: 1) measures/estimates the system state; 2) solves a finite horizon optimal control problem formulated on the system model, performance criterion, operating constraints, and current state; and 3) commands the first element of the optimal control sequence to the actuators.

The direct application of MPC to the PWA model of the vehicle dynamics (9) results in a hybrid MPC controller (hMPC) [17], [18]. The hMPC finite horizon optimal control problem involves continuous and discrete optimization variables, where the first ones select the continuous commands and the second ones encode the PWA system mode. The resulting problem is a mixed-integer program. Because of the complexity of mixed-integer programming algorithms, we further simplify (9) by ignoring the steering dynamics (φ in (4)). The simplified model is discretized in time with sampling period $T_s = 100$ ms

$$x^r(k+1) = A^r_{i(k)} x^r(k) + B^r_{i(k)} u^r(k) + \phi^r_{i(k)} \tag{10a}$$
$$y^r(k) = C^r x^r(k) + D^r u^r(k) \tag{10b}$$
$$i(k) \ : \ H^r_{i(k)} x^r(k) \leq K^r_{i(k)} \tag{10c}$$

where $k \in \mathbb{Z}_{0+}$ is the sampling instant, $x^r = [\alpha_f \ \alpha_r]'$, and $u^r = [\delta \ Y]'$. We then formulate the constraints. For the problem considered here, in order to maintain the system in the region where sufficient lateral force can be developed, we constrain the slip angles as

$$\alpha_{f,\min} \leq \alpha_f(k) \leq \alpha_{f,\max} \tag{11a}$$
$$\alpha_{r,\min} \leq \alpha_r(k) \leq \alpha_{r,\max}. \tag{11b}$$

In order to preserve feasibility, (11) is enforced by soft constraints [21]. In this formulation, the steering angle is actuated only by the AFS system, hence it is constrained in the actuation range of the AFS motor

$$\delta_{\min} \leq \delta(k) \leq \delta_{\max}. \tag{12}$$

The braking torques limits induce constraints on the yaw moment, which, for the maneuvers of interest, are

$$Y_{\min} \leq Y(k) \leq Y_{\max}. \tag{13}$$

Based on model (10) and constraints (11)–(13), the MPC finite horizon optimal control problem at $k \in \mathbb{Z}_{0+}$ is

$$\min_{U^r_N(k)} \sum_{h=0}^{N-1} \|x^r(h+1|k) - \hat{x}(k)\|^2_{Q_x} + \|y^r(h|k) - \hat{y}(k)\|^2_{Q_y} + \|u^r(h|k) - \hat{u}(k)\|^2_{R_u} \tag{14a}$$

s.t.

$$x^r(h+1|k) = A^r_{i(h|k)} x^r(h|k) + B^r_{i(h|k)} u^r(h|k) + \phi^r_{i(h|k)} \tag{14b}$$
$$y^r(h|k) = C^r x^r(h|k) + D^r u^r(h|k) \tag{14c}$$
$$i(h|k) \ : \ H^r_{i(h|k)} x^r(h|k) \leq K^r_{i(h|k)} \tag{14d}$$
$$x^r(0|k) = x^r(k) \tag{14e}$$
$$u_{\min} \leq u^r(h|k) \leq u_{\max} \tag{14f}$$
$$x_{\min} \leq x^r(h|k) \leq x_{\max} \tag{14g}$$
$$h = 0, \ldots, N-1,$$

where N is the horizon, $U^r_N(k) = (u^r(0|k), \ldots, u^r(N-1|k))$ is the control input sequence, $x(k)$ is the measured/estimated state at time k, and $Q_x \geq 0$, $Q_u, Q_y > 0$ are weighting matrices. In (14), $\hat{x} = [\hat{\alpha}_f \ \hat{\alpha}_r]'$, $\hat{u} = [\hat{Y} \ \hat{\delta}]'$, $\hat{y} = \hat{r}$ are the set points for state, input, and output vectors, respectively. Problem (14) is translated into a mixed-integer quadratic program (MIQP), where a quadratic cost is minimized subject to linear constraints, and where some variables are integer-valued. According to the receding horizon mechanism, the first element of the optimizer $U^{r*}_N(k)$ of (14) is used as control input at time k, i.e., $u^r(k) = u^{r*}(0|k)$, and at the following control cycle the procedure is repeated from the newly estimated/measured state.

A. Simulations of the hMPC Controller

The hMPC strategy for vehicle stability control was tested in simulation in a closed loop with a nonlinear vehicle model derived from (1), (2), (6), and (7), which also includes a model of the steering and brake actuators, surface dependency on the tire model [30], and longitudinal dynamics and slip. The simulation model represents the test vehicle in Fig. 1, for which $m = 2050$ kg, $I_z = 3344$ kgm^2, $a = 1.43$ m, and $b = 1.47$ m. The nominal longitudinal velocity is set to $v_x = 15$ m/s (54 km/h), and the nominal surface is

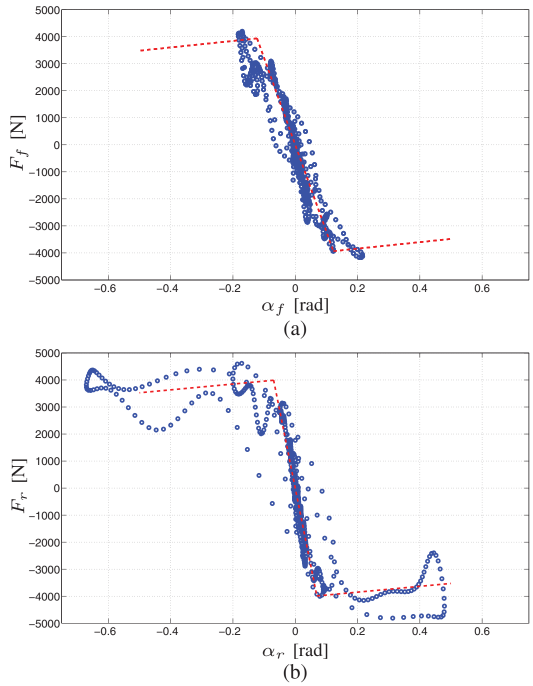

Fig. 4. Experimental tire data (dotted line) and piecewise linear approximation (dashed line) of the tire sideslip angle–force characteristics (2). (a) Front tires. (b) Rear tires.

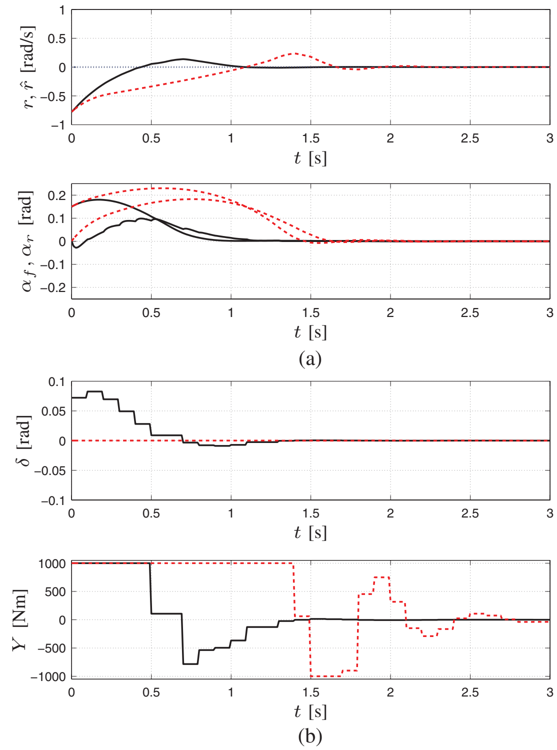

Fig. 5. Time history of states, inputs, and outputs in the stabilization simulation for hMPC with AFS and brakes (solid line), and brakes-only controller (dashed line). (a) Upper plot: yaw rate and target yaw rate (dotted line). Lower Plot: tire slip angles. (b) Upper plot: AFS steering angle. Lower plot: yaw moment from braking.

packed snow ($\mu = 0.45$). The tire forces are identified from a dataset collected on a similar surface using a high-precision localization system and strain gauges installed on the steering rack. Additional details on sensors and tire identification data are given in [30] and [32].

In Fig. 4, the tire data and the chosen PWA approximation are shown. The estimated parameters of the PWA model of the tire forces are $c_f = -3.2 \times 10^4$, $d_f = 1.2 \times 10^3$, and $e_f = -4.0 \times 10^3$ for the front tires, where the saturation angle is $p_f = 0.12$ rad, and $c_r = -5.7 \times 10^4$, $d_r = 1.1 \times 10^3$, and $e_r = -4.0 \times 10^3$ for the rear tires, with saturation angle $p_r = 0.07$ rad. We did not pursue fine optimization of the tire model to investigate the controller robustness to modeling errors.

The bounds in (11)–(13) are set to

$$\alpha_{\mathrm{f,max}} = -\alpha_{\mathrm{f,min}} = 0.3\mathrm{rad},\ \ \alpha_{\mathrm{r,max}} = -\alpha_{\mathrm{r,min}} = 0.275\mathrm{rad},$$
$$\delta_{\max} = -\delta_{\min} = 0.35\mathrm{rad},\ \ Y_{\max} = -Y_{\min} = 1000\ \mathrm{Nm}.$$

Note that the slip angles are allowed to stay in saturation.

The value of the driver-requested RWA, δ_{drv} [rad], is computed from the driver input on the steering wheel (SWA), δ_{SWA} [rad], by multiplying the SWA by the steering gear ratio, g_{col}, i.e., $\delta_{\mathrm{drv}} = g_{\mathrm{col}}^{-1}\delta_{\mathrm{SWA}}$. In the hMPC controller, the steering angle is actuated uniquely by the AFS motor. Hence, δ_{drv} is used only for calculating the target slip angles and yaw rate, by computing the equilibrium of (9) for the current longitudinal velocity v_x, $\delta = \delta_{\mathrm{drv}}$, $Y_M = 0$, and $\varphi = 0$, while assuming nonsaturated tires. For the following simulations, the horizon $N = 3$ is used in (14).

The first simulation test, shown in Fig. 5, illustrates the capabilities of the control strategy in recovering from a loss of stability, i.e., from an initial condition on one of the unstable open-loop trajectories in Fig. 3, where the rear tires are saturated, but the front tires are not. In a rear-wheel drive (RWD) vehicle, this may be caused, for instance, by an excessive acceleration on a low friction surface while negotiating a turn. We compare the performance of the controller that uses AFS and differential braking with a controller that uses only brakes and does not perform prediction. Such a controller is more similar to currently implemented ESC algorithms [6], [7], which actuate only the brakes reactively rather than predictively. With these simulations, we also aim at showing the potential benefits of coordinating AFS and brakes, instead of using only the brakes.

The time history of the slip angles in the test is shown in Fig. 5(a). The hMPC controller that uses AFS and brakes achieves faster convergence to the equilibrium. Fig. 5(b) shows that by using AFS the activity of the brakes is significantly reduced, and so will be the perturbation to the longitudinal dynamics, which may disturb the driver because of the associated aggressive decelerations.

Fig. 6 shows the trajectory of tire slip angles in the phase plane. When both AFS and brakes are used, the maximum value of α_r is reduced and the trajectory remains significantly closer to the origin. According to Fig. 3, the vehicle dynamics becomes particularly unstable when the angles are large and $\alpha_r \geq \alpha_f$. Hence, the coordination of AFS and brakes appears to improve vehicle stability.

In a second series of simulations, we analyze the robustness to parameter variations with respect to the ones used in

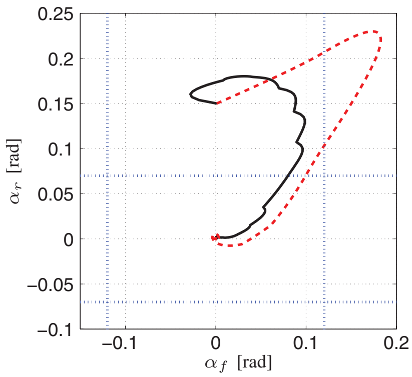

Fig. 6. Phase plane trajectory of the tire slip angles in the stabilization simulations for AFS and brakes hMPC (solid line), and brakes-only controller (dashed line). The saturation angles are also shown (dotted line).

the prediction model (10), referred to as "nominal," in what follows. While several parameters can change as a result of the variability of the vehicle operating conditions, we report here the simulations for those that resulted to be more critical, i.e., the longitudinal velocity (v_x), the road friction coefficient (μ), and the peak tire force angle (p_j, $j \in \{f, r\}$). We evaluate the robustness in a tracking test that simulates a step-steering, i.e., the vehicle is requested to achieve and maintain a constant yaw rate, starting from straight driving. The target yaw rate behavior is generated from nominal conditions ($\bar{v}_x = 15$ m/s, $\bar{\mu} \approx 0.45$) for a step change from 0 to 60 degrees in SWA.

In Fig. 7(a), we show the target yaw rate as well as the time histories of the yaw rate and of the rear tire slip angle (the critical angle for detecting the loss of stability) for the cases of nominal longitudinal velocity $\bar{v}_x = 15$ m/s (dash, red), and for the cases of $v_x = \bar{v}_x \times \{0.6, 0.8, 1.2, 1.4, 1.6\}$ in increasingly dark color (from light blue to black). When the velocity is smaller than the nominal one, only a steady-state error is induced. When the velocity is larger than the nominal one, first a steady-state error is induced, and then stability losses may occur. The latter only happens for large variations with respect to the nominal value. In Fig. 7(b), we show the target yaw rate (dotted) and the time histories of the yaw rate and of the rear tire slip angle for the nominal case $\mu = \bar{\mu}$, the value used in the hMPC tire force model (dash, red), and for $\mu = \bar{\mu} \cdot \{1.5, 0.75, 0.5, 0.4\}$, in increasingly dark color (from light blue to black). If μ is only slightly different from the nominal value, only a steady-state error occurs, while if μ is significantly smaller than the nominal value, stability losses may occur. The latter only happens for extremely large errors in the parameters, e.g., when the actual μ corresponds to polished ice. In Fig. 7(c), we show the time histories of the yaw rate and of the rear tire slip angle for the nominal tire force peak angle $\bar{p}_j$, $j \in \{f, r\}$ (dash, red) and for the cases where $p_j = \{1.2, 0.9, 0.8, 0.7\}\bar{p}_j$, $j \in \{f, r\}$, in increasingly dark color (from light blue to black). The tire force continuity is preserved by adjusting the tire peak force. For values of p_j, $j \in \{f, r\}$, larger than in the nominal case, the controller keeps the slip angles smaller, and the stabilization is faster. When p_j, $j \in \{f, r\}$, is smaller than in the nominal case, the slip angles grow larger and the stabilization takes longer, but stability is maintained. Since the initial condition is the same

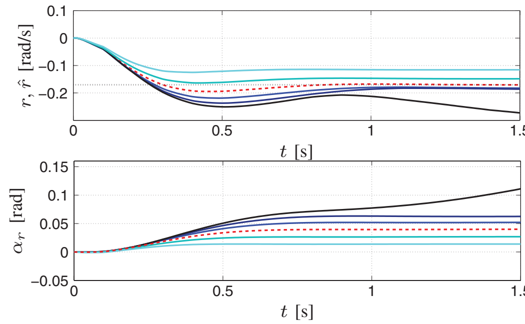

(a)

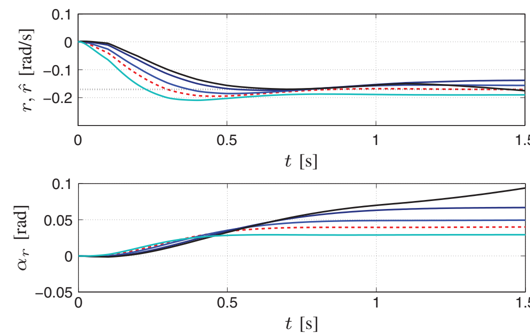

(b)

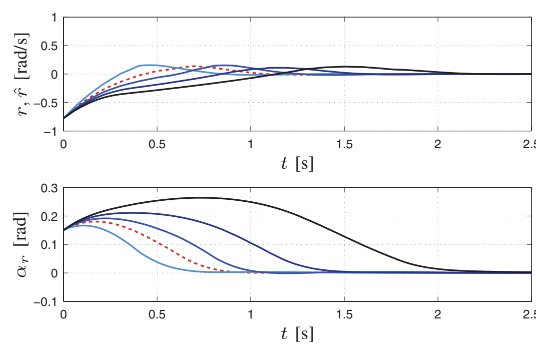

(c)

Fig. 7. Time history of yaw rate and rear tire slip angle in the robustness simulations. Nominal condition (dashed line), and non-nominal conditions (solid line). (a) Robustness to longitudinal velocity variations. Upper plot: yaw rate, target yaw rate (dotted line). Lower plot: rear tire slip angle. (b) Robustness to μ variations. Upper plot: yaw rate, target yaw rate (dotted line). Lower plot: rear tire slip angle. (c) Robustness to peak force angle variations. Upper plot: yaw rate, target yaw rate (dotted line). Lower plot: rear tire slip angle.

in all the tests but the tire forces are different, the smaller the saturation angle, the more challenging the initial condition.

The robustness tests show that reasonable ranges of parameter variations can be tolerated by the controller. In order to ensure high performance and robustness across the whole operating range, controller scheduling can be applied, as is common practice, using different prediction models for different conditions. However, the range where the controller operates robustly is sufficient for the tests discussed in this paper. Next, we develop a controller for implementation in automotive-grade ECUs.

IV. Switched Model Predictive Control Design

The hMPC controller solves every control cycle problem (14), which is a MIQP. Although satisfactory performance is achieved, in terms of stability, yaw rate tracking, and robustness to parameter variations, the memory and chronometric requirements of mixed-integer programming are too large for implementation in automotive-grade ECUs at the desired sampling rate (10–20 Hz). Even if synthesized in explicit form [33], the controller is still too complex in terms of memory occupancy and worst case computations required [1].

Explicit hMPC is complex because a PWA control law is computed for each sequence of PWA modes along the prediction horizon. Given s modes and horizon N, s^N control laws are computed and they cannot be merged into a single PWA function [33]. Thus, the s^N laws must be stored together with their value functions, the functions that describe the optimal cost as a function of the state x. At each control cycle, all the s^N laws are evaluated for the current value of x, and the one with the smallest value function is selected. Symmetry of (10) can be used to reduce the modes to 4, so that for $N = 3$, 64 PWA control laws are obtained, for more than 5000 regions [1].

The simulations in Section III-A have shown that the system in closed loop with the hMPC controller exhibits relatively few mode switches, and that almost no multiple switches occur over short periods (0.5–1 s). As a consequence, one can consider as prediction model the PWA system, where the mode is maintained constant along the prediction horizon and the constraints that enforce the PWA partitions are ignored after the first step. Referring to (14), this means $i(h|k) = i(0|k)$ for all $h = 1, \ldots, N-1$, and (14d) is enforced only for $h = 0$. Thus, the feasible mode sequences are reduced to s, at the price of neglecting the effects of mode switches during the prediction horizon. Furthermore, because of (14d), for an assigned $x(k)$ only one value $i(0|k) \in \mathcal{I}$ exists such that (14d) is satisfied for $h = 0$. Hence, $i(k)$ is uniquely assigned by the state, so that (14d) does not need to be enforced and the number of constraints is significantly reduced. Let

$$\gamma_{\text{MPC}}(i, x), \quad i \in \mathcal{I} \tag{15}$$

be the MPC control law obtained by (14), where $i(h|k) = i$ for all $h = 0, \ldots, N-1$, and (14d) is removed. Since for a fixed $i \in \mathcal{I}$, (15) is applied only for the states x such that $H_i x \le K_i$, we call it the *local MPC law*. The sMPC algorithm operates as follows. Given $x(k)$: 1) find $i(k)$ such that $H_{i(k)}x(k) \le K_{i(k)}$ and 2) select as command $u(k) = \gamma_{\text{MPC}}(i(k), x(k))$.

Remark 2: The PWA polyhedral partition (9c) does not depend on the input $u(k)$. Thus, given $x(k)$, there is only one feasible mode $i \in \mathcal{I}$. In the case of general PWA partitions, $H_{i(k)}x(k)+M_{i(k)}u(k) \le K_{i(k)}$, multiple MPC laws might need to be evaluated, and the control input selected as the one associated with the smallest value function. The solution of s QPs is generally simpler than the solution of the MIQP (14) modeling s^N mode sequences [34].

A. Switched MPC Prediction Model

The complexity of sMPC is reduced with respect to hMPC, hence we use as plant prediction model (8) discretized in time with sampling period $T_s = 50$ ms

$$x(k+1) = A_{i(k)}x(k) + B_{i(k)}u(k) + \phi_{i(k)} \tag{16a}$$
$$y(k) = C_{i(k)}x(k) \tag{16b}$$
$$i(k) : H_{i(k)}x(k) \le K_{i(k)} \tag{16c}$$

where $k \in \mathbb{Z}_{0+}$ is the sampling instant. In (16), the steering rate is a control input, hence constraints on AFS motor rate can be enforced.

Since the final objective is the design of a driver steering assist system, we decompose the total RWA δ into the components due to driver steering, δ_{drv}, and to AFS, δ_{AFS} [rad]. For the considered AFS architecture

$$\delta(k) = \delta_{\text{drv}}(k) + \delta_{\text{AFS}}(k). \tag{17}$$

Similarly, the steering rate $\dot{\delta} = \varphi$ can be decomposed as

$$\varphi = \varphi_{\text{drv}}(k) + \varphi_{\text{AFS}}(k) \tag{18}$$

where $\dot{\delta}_{\text{drv}}(k) = \varphi_{\text{drv}}(k)$, and $\varphi_{\text{AFS}}(k) = \dot{\delta}_{\text{AFS}}(k)$.

While more advanced models have been tested for driver steering prediction, for instance, constant driver steering rate and first order driver steering dynamics, a constant driver steering angle prediction is used in this paper. Note that closed-loop models of the driver are not possible here, since the desired path is not known, as in ESC systems. Thus, for $h = 0, \ldots, N-1$ in the prediction model $\delta_{\text{drv}}(h|k) = \delta_{\text{drv}}(k)$, and as a consequence $\varphi_{\text{drv}}(h|k) = 0$, $[u(h|k)]_1 = \varphi_{\text{AFS}}(h|k)$.

In order to increase the robustness with respect to model imperfections, we generate the yaw rate reference by

$$\hat{r}(k) = \frac{v_x(k)}{L + \kappa v_x(k)^2}\delta_{\text{drv}}(k) \tag{19}$$

where $L = (a + b)$. The reference yaw rate (19) is a static function of the driver steering angle and the current longitudinal velocity [6]. The parameter κ, called understeering gain [28], embeds information on the tire force curves and the surface friction, and it can be either constant or updated online. Since by (19) the yaw rate reference is a function of the driver steering and of the longitudinal velocity only, both of which are assumed constant in prediction, the yaw rate reference is also constant in prediction.

Remark 3: Equation (19) can be exploited to modify the steady-state vehicle cornering behavior. By introducing a mismatch between κ in (19) and the current surface, the controller will converge to a nonzero value δ_{AFS} at steady state, thereby increasing/decreasing the steady-state yaw rate with respect of what would be produced without AFS.

By adding driver input δ_{drv} and yaw rate reference $\hat{r}$ to (16), the ith mode prediction model is

$$x_p(k+1) = A_i^p x_p(k) + B_i^p u_p(k) + \Gamma^p \phi_i^p \tag{20a}$$
$$y_p(k+1) = C^p x_p(k) \tag{20b}$$
$$i : [H_i \ 0]x^p(k) \le K_i(k) \tag{20c}$$

$$A_i^p = \begin{bmatrix} A_i & [A_i]^3 & 0 \\ 0 & 1 & 0 \\ 0 & 0 & 1 \end{bmatrix}, \quad B_i^p = \begin{bmatrix} B_i \\ 0 \\ 0 \end{bmatrix}$$

$$\Gamma^p = \begin{bmatrix} I \\ 0 \end{bmatrix}, \quad C^p = [\, C \ [C]^3 \ -1 \,]$$

where $x_p = [\alpha_f\ \alpha_r\ \delta_{\text{AFS}}\ \delta_{\text{drv}}\ \hat{r}\ ]'$, $u_p = [\varphi_{\text{AFS}}\ Y]'$, $\phi_i^p = \phi_i$, $i \in \mathcal{I}$, and $y_p = r - \hat{r}$, i.e., the tracking error.

B. Cost Function and Constraints

By using φ_{AFS} as control input, we can include constraints on AFS motor angle and angular rate. Owing to the mechanical design and physical limits of the AFS motor, we enforce

$$\delta_{\min} \leq \delta_{\text{AFS}}(k) \leq \delta_{\max} \tag{21}$$

$$\varphi_{\min} \leq \varphi_{\text{AFS}}(k) \leq \varphi_{\max}. \tag{22}$$

Limits on the total steering angle [i.e., (12)], are instead neglected in the controller design to reduce the controller complexity, since these are not reached in normal driving.

The objective of the driver-assist steering system is to track the desired yaw rate while avoiding the slip angles to exceed the linear region of the tire curve (i.e., to avoid the vehicle dynamics to be in the unstable regions) for long periods, since this is not appropriate for normal driving. The desired behavior is encoded by the cost function

$$J = \sum_{k=0}^{N-1} q_i^{(r)}(r(k) - \hat{r}(k))^2 + q_i^{(\alpha_f)}\alpha_f(k)^2 + q_i^{(\alpha_r)}\alpha_r(k)^2 + q_i^{(Y)}Y(k)^2 + q_i^{(\varphi)}\varphi_{\text{AFS}}(k)^2 \tag{23}$$

where $q_i^{(r)}, q_i^{(\alpha_f)}, q_i^{(\alpha_r)}, q_i^{(Y)}$, and $q_i^{(\varphi)} \in \mathbb{R}_{0+}$, for all $i \in \mathcal{I}$, are the tuning weights that trade off the different objectives.

C. Switched MPC Synthesis

The number of local MPC control laws to be computed can be reduced by considering that the angle–force relations in (2) are symmetric and the equations for positive and negative saturation have the same linear coefficient but different affine terms ϕ_i. In the sMPC controller, the affine term in (20) is assigned at the initial prediction step and remains constant along the prediction horizon. Thus, we modify (20) including the affine term ϕ_i in the state vector as

$$x_s(k+1) = A_i^s x_s(k) + B_i^s u_s(k) \tag{24a}$$

$$A_i^s = \begin{bmatrix} A_i^p & \Gamma^p \\ 0 & I \end{bmatrix},\quad B_i^s = \begin{bmatrix} B_i^p \\ 0 \end{bmatrix},\quad x_s(k) = \begin{bmatrix} x_p(k) \\ \phi(k) \end{bmatrix} \tag{24b}$$

where $u_s(k) = u_p(k)$, and $\phi(k) = \phi_{i(k)}^p$. Since $\phi(k)$ is included as a parameter in $x_p(k)$, only four dynamical models have to be considered in the sMPC design, $i \in \mathcal{I} = \{1, \ldots, 4\}$, thereby generating only four different local MPC laws. The four modes represent linear and saturated tire force dynamics for front and rear tires. Negative and positive saturation are differentiated by the affine term $\phi(k)$, which is a parameter in the initialization of the MPC problem and is maintained constant along the prediction horizon.

By collecting prediction model (24), cost function (23), and constraints (11), (13), (21), (22), we design the local MPC laws (15), for all $i \in \mathcal{I}$. For each mode $i \in \mathcal{I}$, the sMPC optimization problem is

$$\min_{U_N(k)} \sum_{h=0}^{N-1} \|x_s(h+1|k)\|_{Q_i}^2 + \|u_s(h|k)\|_{R_i}^2 \tag{25a}$$

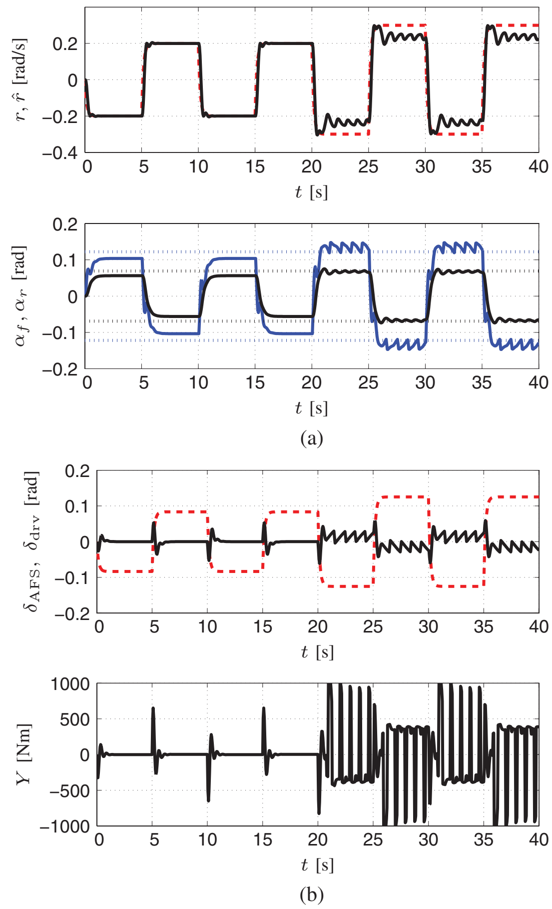

Fig. 8. Simulation of a slalom maneuver. (a) Upper plot: yaw rate reference (dashed line) and yaw rate (solid line). Lower plot: slip angles (solid line) and saturation angles (dotted line). (b) Upper plot: driver steering angle (dashed line) and AFS actuator steering angle (solid line). Lower plot: differential braking yaw moment.

$$\text{s.t.}\quad x_s(h+1|k) = A_i^s x_s(h|k) + B_i^s u_s(h|k) \tag{25b}$$

$$u_{\min} \leq u_s(h|k) \leq u_{\max},\ \ h = 0, \ldots, N-1 \tag{25c}$$

$$x_{\min} \leq x_s(h|k) \leq x_{\max},\ \ h = 1, \ldots, N_y \tag{25d}$$

$$u_s(h|k) = 0,\ \ h = N_u, \ldots, N-1 \tag{25e}$$

$$x_s(0|k) = [x(k)'\ \delta_{\text{drv}}(k)\ \hat{r}(k)\ \phi(k)']' \tag{25f}$$

where $U_N(k) = (u_s(0|k), \ldots, u_s(N-1|k))$, and the prediction horizon (N) may be different from the state constraints horizon (N_y), i.e., the number of steps along which (11) is enforced, and from the control horizon (N_u), i.e., the number of free control moves to be chosen. Choosing N_y and N_u smaller than N reduces the controller complexity while maintaining the prediction capabilities. Since the system mode is fixed, (25) results in a quadratic program that has a polynomial complexity [35], as opposed to the exponential complexity of MIQPs [34]. The output term of (23) can be included in (25a) as $x_s' Q_i x_s = x_s(C^{s\prime}\bar{Q}_{y,i}C^s + \bar{Q}_{x,i})x_s$, and $C^s = [C^p\ 0]$, for $i \in \mathcal{I}$.

The sMPC feedback law can be explicitly computed. Problem (25) is a quadratic program that can be solved as a function of $x(k)$ by multiparametric programming [16]. In this way, for each mode $i \in \mathcal{I}$, the local MPC law is the PWA static state feedback

$$\gamma_{\rm MPC}(i, x_s) = F_j^i x_s + G_j^i \tag{26}$$

$$j : H_j^i x_s \leq K_j^i \tag{27}$$

where $j \in \mathcal{J}_i$, $\mathcal{J}_i = \{1, \dots, s_i\}$, and s_i is the number of regions of the MPC law associated to the ith mode.

The global sMPC law is obtained by combining (26) for all $i \in \mathcal{I}$ with the mode selection inequalities in (16c). The result is the PWA function

$$u_s = F_j^i x_s(k) + G_j^i \tag{28a}$$
$$i, j \ : \ [H_i \ 0] x_s(k) \leq K_i \tag{28b}$$
$$H_j^i x_s(k) \leq K_j^i, \tag{28c}$$

where (28b) is the controller selection rule and (28c) is the region selection rule. As a consequence, the closed loop is described by the PWA system

$$x_s(k+1) = (A_i^s + B_i^s F_j^i) x_s(k) + G_j^i \tag{29a}$$
$$i, j \ : \ [H_i \ 0] x_s(k) \leq K_i \tag{29b}$$
$$H_j^i x_s(k) \leq K_j^i, \tag{29c}$$

where $i \in \mathcal{I}$, $j \in \mathcal{J}_i$, and whose stability can be studied globally via quadratic or piecewise quadratic Lyapunov functions [27]. A local stability analysis [36] can be developed by identifying the control law $\bar{\imath}$ and the region $\bar{\jmath}$ that contain the equilibrium, and then evaluating the eigenvalues of $(A_{\bar{\imath}}^s + B_{\bar{\imath}}^s F_{\bar{\jmath}}^{\bar{\imath}})$. Let the maximum absolute value of the eigenvalues of $(A_{\bar{\imath}}^s + B_{\bar{\imath}}^s F_{\bar{\jmath}}^{\bar{\imath}})$ be not larger than 1 (with full geometric multiplicity). Let $\mathcal{X}_{\rm PI}$ be the largest positive invariant set contained in $\bar{\mathcal{X}} = \{x_s \in \mathbb{R}^n : [H_{\bar{\imath}} \ 0] x_s \leq K_{\bar{\imath}}, H_{\bar{\jmath}}^{\bar{\imath}} x_s \leq K_{\bar{\jmath}}^{\bar{\imath}}\}$ for dynamics $x_s(k+1) = (A_{\bar{\imath}}^s + B_{\bar{\imath}}^s F_{\bar{\jmath}}^{\bar{\imath}}) x_s(k) + G_{\bar{\jmath}}^{\bar{\imath}}$. Then, (29) is stable in $\mathcal{X}_S \subseteq \mathbb{R}^n$ such that $\mathcal{X}_S \supseteq \mathcal{X}_{\rm PI}$.

V. Simulation and Experimental Results

The controller designed in Section IV is evaluated in simulations and experimental tests in different maneuvers.

A. Simulation Results

Because of the reduced computational load of the sMPC algorithm, we could implement the control strategy with horizons $N = 10$, $N_u = 3$, and $N_y = 3$. The bounds on the slip angles and on the yaw moment by differential braking are the same as in Section III-A. The bounds on the AFS motor angle and angular rate in (21) and (22) are set to

$$\delta_{\max} = -\delta_{\min} = 0.175 \text{ rad}, \ \ \varphi_{\max} = -\varphi_{\min} = 0.5 \text{ rad/s}.$$

We have calibrated the weights in (23) to trade off between tracking performance, robustness to the model approximations, and reduced switching frequency on the border of the linear region. In particular, we have set $q_i^{(\alpha_j)} = 0$, $j \in \{f, r\}$ for all $i \in \mathcal{I}$ such that α_j is in the linear tire region ($|\alpha_j| \leq p_j$), while we set $q_i^{(\alpha_f)} = 10^4$, $q_i^{(\alpha_r)} = 3 \times 10^4$, elsewhere. The changes in the weights enforce the different objectives in the different tire force regions. When the vehicle is in the linear tire force region the objective is to track the yaw rate, possibly with minimum use of differential braking since this perturbs the longitudinal dynamics, while in the tire saturation region it becomes of primary importance to return to the linear region, possibly by using also the brakes.

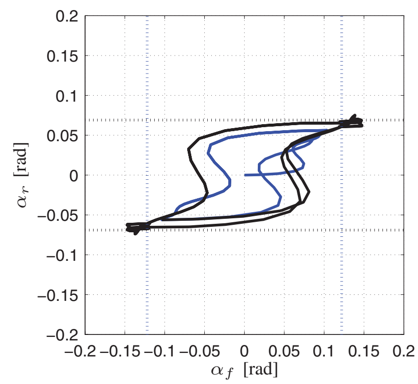

Fig. 9. Phase plane plot of the slip angles for achievable (blue) and unachievable (black) target yaw rate in the simulation of a slalom maneuver.

The sMPC synthesized in explicit form (28) has 273 regions, and its evaluation has worst case upper bound of 5×10^4 atomic operations per second, which is in the range of capabilities of currently available automotive ECUs [36]. In simulations and experimental tests, the average computation load was approximately 8% of the worst case. The C-code of this class of controllers has been demonstrated to be compatible with production-like automotive ECUs in [37]. For the closed-loop dynamics (29), we have verified local asymptotic stability since in the linear region, $\max_\ell |\lambda_\ell| = 0.83$, where $\{\lambda_\ell\}_\ell$ is the set of closed-loop system eigenvalues.

Before testing the controller in the vehicle, we have qualitatively evaluated the performance in simulation, using the same continuous time nonlinear simulation model as in Section III. In Fig. 8 we show a simulated slalom maneuver where the driver steering changes every 5 s by step steering. For the first 20 s the desired yaw rate is achievable and, since the steering-to-yaw rate gain of (19) is tuned to match that of the simulation model, the vehicle yaw rate converges to the set point, with the control system assisting the driver during the transients. After 20 s in the simulation, the amplitude of the desired yaw rate signal is increased, resulting in a target yaw rate that is not achievable for the available tire force. In this case, the driver-assist system stabilizes the vehicle to achieve a close feasible yaw rate. The controller produces a behavior similar to a limit cycle between the linear and saturation regions of the tire force, see Fig. 8. The trajectories in the (α_f, α_r) phase plane are shown in Fig. 9, where the color changes after 20 s in the simulation to highlight the difference between feasible and infeasible yaw rate tracking conditions.

B. Experimental Results

The sMPC controller with the parameters described in Section V-A is evaluated on the protoype RWD vehicle (see Fig. 1) whose parameters have been introduced in Section III and which is equipped with a 4.2-L V8 engine and a six-speed automatic transmission. The controller and the drivers for the

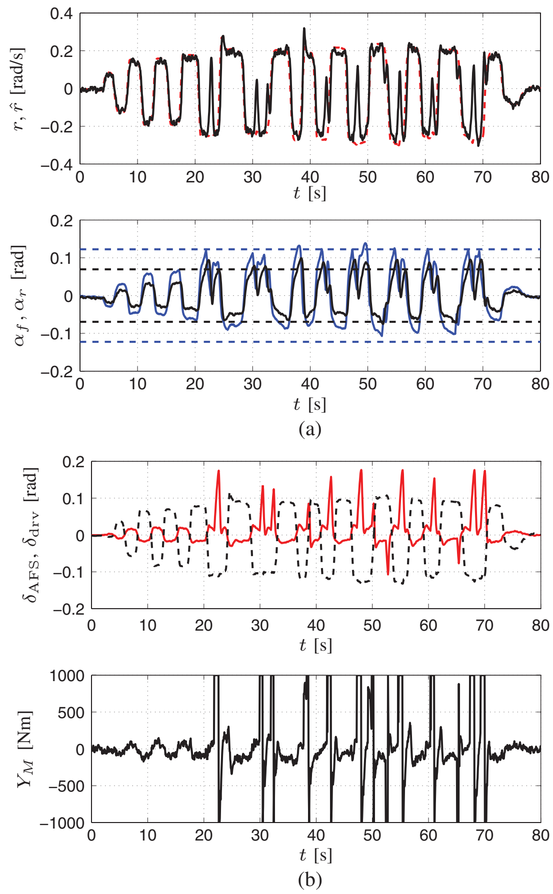

Fig. 10. Experimental validation of the control strategy in a slalom test. (a) Upper plot: yaw rate reference (dashed line) and yaw rate (solid line). Lower plot: slip angles (solid line) and saturation angles (dashed line), front in blue, rear in black. (b) Upper plot: AFS actuator steering angle (solid line), driver steering angle (dashed line). Lower plot: yaw moment.

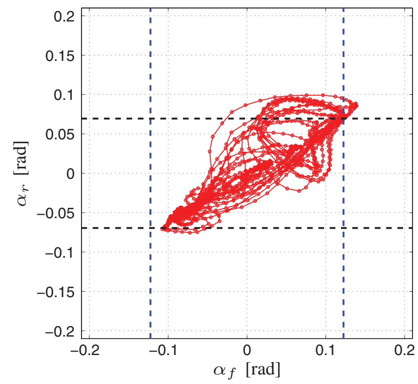

Fig. 11. Phase plane plot of the tire slip angles in the slalom test.

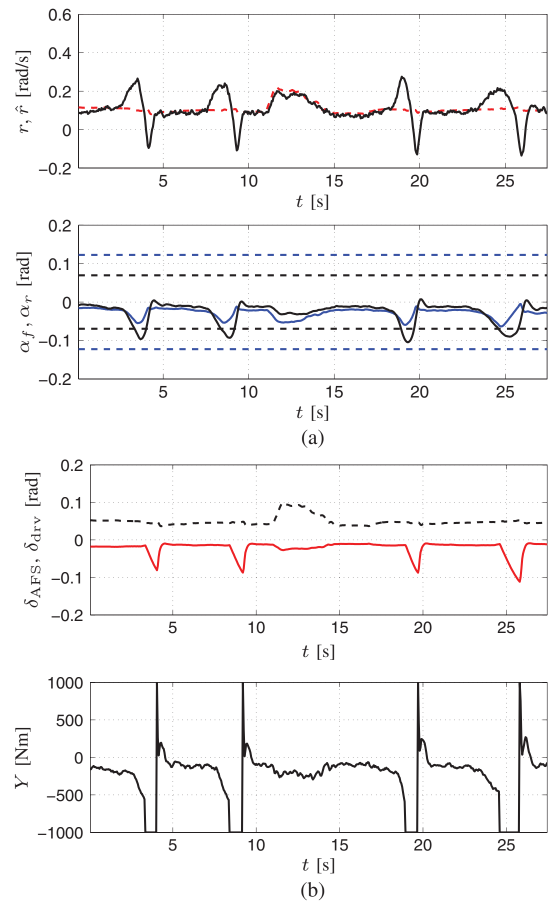

Fig. 12. Experimental validation of the control strategy in a stability recovery test. (a) Upper plot: yaw rate reference (dashed line) and yaw rate (solid line). Lower plot: slip angles (solid line) and saturation angles (dashed line), front in blue, rear in black. (b) Upper plot: AFS actuator steering angle (solid line), driver steering angle (dashed line). Lower plot: yaw moment from differential braking.

AFS motor and for the brake torque actuation are executed in a dSPACE Autobox system, equipped with a DS1005 processor board and a DS2210 I/O board. The vehicle sensing system includes encoders to measure the SWA and the AFS actuator angle, and an Oxford Technical Solution RT3000 localization system. The RT3000 is equipped with two global positioning system antennas and an inertial measurement unit with three accelerometers and three angular rate sensors. A Kalman filter is executed in a local DSP for sensor fusion. The RT-3000 provides the controller the yaw rate and the longitudinal and lateral velocities, from which the slip angles are estimated by low-pass filtering (1). The yaw rate measured by the RT-3000 is also used as "ground truth" to evaluate the closed-loop performance. In normal vehicles where advanced sensors are not available, the slip angles can be estimated using methods available in the literature (see [38] and the references therein). The yaw moment command issued by the MPC controller is translated into braking torques achieving such a yaw moment by using the logics in [26]. The experimental tests reported here have been executed on icy/packed/soft snow, $\mu \in [0.35, 0.55]$, for longitudinal velocity $v_x \in [40, 75]$ km/h. The controller has also been tested on surfaces with $\mu \in [0.20, 0.70]$.

The first test, whose results are reported in Fig. 10, is a slalom maneuver, similar to the sequence of step-steering simulated in Section V-A. The driver-requested yaw rate is tracked until the slip angles grow beyond the saturation angle. When this happens, the controller countersteers to stabilize the vehicle. The impact of the recovery action on the yaw rate is more evident than what is seen in simulation because of effects such as the uncertainty and variability of the surface friction, the variations in the velocity, and the tire force hysteresis, which can also be noticed in Fig. 4. A similar behavior was

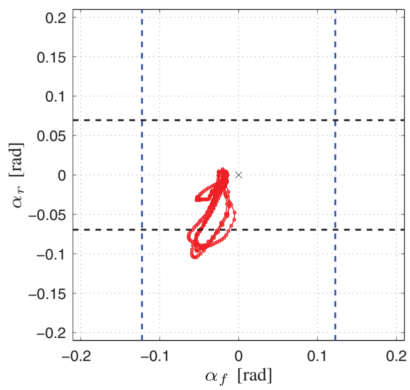

Fig. 13. Phase plane plot of the tire slip angles in the stability recovery test.

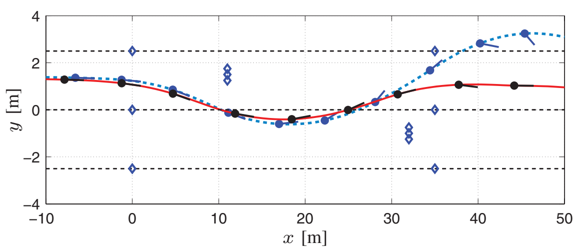

Fig. 14. Trajectories in a double-lane-change experiment with active (solid line) and inactive (dashed line) control. Vehicle center of mass (circle) and heading (line).

noticed in simulations with imperfect tire models. Note that a light countersteering action is present at steady state, compensating for the difference between the actual friction and that used in the computation of the understeering gain κ in (19). By changing κ in (19), a steady-state pro-steering action can be obtained, as discussed in Remark 3. Fig. 11 shows the phase plane plot of the tire slip angles, where it is demonstrated that the controller is rapidly pushing the slip angles back in the linear region, when these move outside. The trajectory to bring the rear tire sideslip angle back in the linear region is slightly different from that in the simulation, moving for longer time along the surface $\alpha_r = p_r$. This is caused by the above-mentioned uncertainties and the dynamics not captured in the bicycle model. However, this does not affect the stabilization capabilities.

Fig. 12 shows a vehicle stabilization test where, while driving in circle at an approximately constant yaw rate, drift is induced by aggressive acceleration. The drift events are shown by the positive yaw rate peaks at approximately 8, 13, 18, and 23 s. For $t \in [11, 15]$ s, the driver adjusts the trajectory with a smooth maneuver, and the system does not intervene. When drifts occur, the driver-assist system actuates AFS and brakes to return the vehicle to a stable condition. Then, yaw rate tracking is resumed. Fig. 13 shows the tire slip angle phase plot for this test.

As the last test, we show a double-lane-change maneuver where a trained, yet nonprofessional, driver executes the double-lane change with and without driver-assist system at approximately 50 km/h entry speed. The trajectories for the cases where the stability control is active and inactive are reported in Fig. 14, which shows that the maneuver is completed successfully when the system is active (solid line), while it is not completed when the system is inactive (dash line). The time histories of states, inputs, and outputs are reported in Fig. 15.

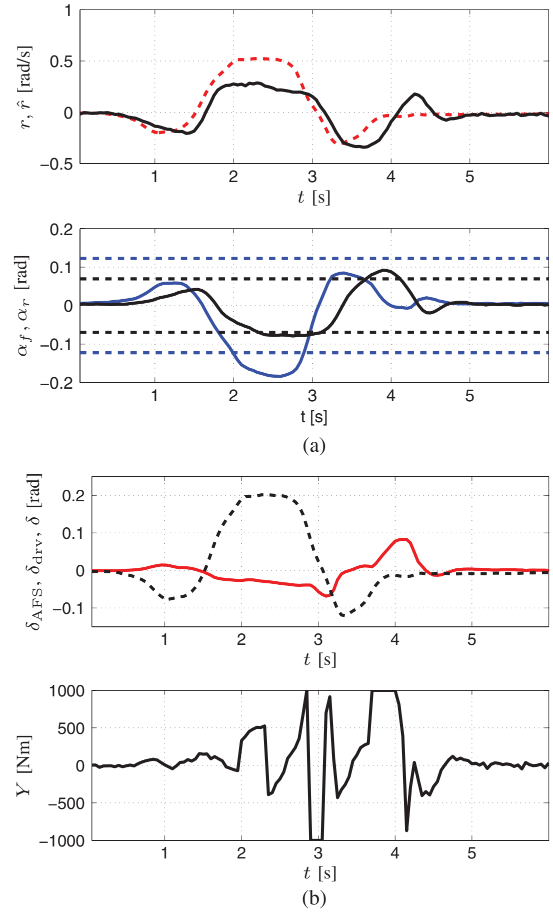

Fig. 15. Experimental validation of the control strategy in the double-lane-change test with sMPC. Time history of states, inputs, and outputs. (a) Upper plot: yaw rate reference (dashed line) and yaw rate (solid line). Lower plot: slip angles (solid line) and saturation angles (dashed line). Front tire data in blue, rear in black. (b) Upper plot: AFS actuator steering angle (solid line), driver steering angle (dashed line). Lower plot: yaw moment from differential braking.

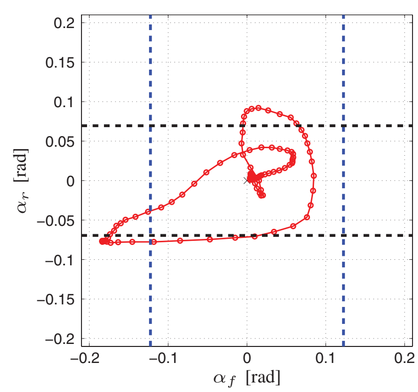

Fig. 16. Phase plane plot of the tire slip angles in the double-lane-change test.

In Fig. 15 one can see that the controller maintains the rear tire slip angle close to the peak level in the interval [2.3, 3] s by using the brakes and only a light countersteering. Excessive countersteering is avoided not to excessively deteriorate the yaw rate tracking performance. In the subsequent time interval, the controller uses both the actuators to improve the yaw rate tracking and to stabilize the vehicle at the end of the maneuver. In fact, after $t = 4$ s the controller stabilizes the vehicle without any intervention from the driver. The tire slip angle phase plot for this test is shown in Fig. 16, where one can see that the controller maintains the rear tire close to the saturation angle, i.e., at the peak force.

VI. Conclusion

In this paper, we have presented the design of a control strategy to coordinate AFS and differential braking to improve vehicle yaw stability and cornering control. By formulating the vehicle dynamics in the tire slip angle domain and approximating the tire forces by PWA functions, the vehicle dynamics was modeled as a PWA system. We have proposed a sMPC strategy that can execute on automotive-grade ECUs, and tested it in different maneuvers and in different conditions. The control algorithm is currently being extended by including adaptation to variations in μ without gain scheduling the explicit control law, by leveraging the special structure of the sMPC controller, and in particular the affine terms ϕ_i and the switching conditions (28b). Also, techniques for improving the driver–controller interaction, especially by reducing the steering wheel feedback torque cancellation due to the AFS motor actuation, and improved driver prediction models are under development.

Acknowledgment

The authors would like to thank D. Hrovat, M. McConnell, and many other colleagues at Ford, for test driving the prototype vehicle and providing useful feedback and suggestions.

References

[1] D. Bernardini, S. Di Cairano, A. Bemporad, and H. Tseng, "Drive-by-wire vehicle stabilization and yaw regulation: A hybrid model predictive control design," in *Proc. 48th IEEE Conf. Decision Control*, Shanghai, China, 2009, pp. 7621–7626.

[2] S. Di Cairano, H. Tseng, D. Bernardini, and A. Bemporad, "Steering vehicle control by switched model predictive control," in *Proc. 6th IFAC Symp. Adv. Autom. Control*, Munich, Germany, 2010, pp. 1–6.

[3] S. Di Cairano and H. Tseng, "Driver-assist steering by active front steering and differential braking: Design, implementation and experimental evaluation of a switched model predictive control approach," in *Proc. 49th IEEE Conf. Decision Control*, Atlanta, GA, Dec. 2010, pp. 2886–2891.

[4] C. Farmer, "Effect of electronic stability control on automobile crash risk," *Traffic Injury Prevent.*, vol. 5, no. 4, pp. 317–325, Dec. 2004.

[5] A. Lie, C. Tingvall, M. Krafft, and A. Kullgren, "The effectiveness of electronic stability control (ESC) in reducing real life crashes and injuries," *Traffic Injury Prevent.*, vol. 7, no. 1, pp. 38–43, 2006.

[6] H. Tseng, B. Ashrafi, D. Madau, T. Brown, and D. Recker, "The development of vehicle stability control at Ford," *IEEE/ASME Trans. Mech.*, vol. 4, no. 3, pp. 223–234, Sep. 1999.

[7] E. Liebemann, K. Meder, J. Schuh, and G. Nenninger, "Safety and performance enhancement: The Bosch electronic stability control (ESP)," in *Proc. SAE Convergence*, Detroit, MI, 2004, no. 2004-21-0060, pp. 1–9.

[8] J. Ackermann, "Robust control preventing car skidding," *IEEE Control Syst. Mag.*, vol. 17, no. 3, pp. 23–31, Jun. 1997.

[9] E. Ono, K. Takanami, N. Iwama, Y. Hayashi, Y. Hirano, and Y. Satoh, "Vehicle integrated control for steering and traction systems by μ-synthesis," *Automatica*, vol. 30, no. 11, pp. 1639–1647, Nov. 1994.

[10] B. Guvenc, T. Acarman, and L. Guvenc, "Coordination of steering and individual wheel braking actuated vehicle yaw stability control," in *Proc. IEEE Intell. Veh. Symp.*, Jun. 2003, pp. 288–293.

[11] K. Koibuchi, Y. Masaki, Y. Fukada, and I. Shoji, "Vehicle stability control in limit cornering by active braking," in *Proc. SAE World Congr.*, Detroit, MI, 1996, no. 960487.

[12] E. Ono, S. Hosoe, D. Hoang, and S. Doi, "Bifurcation in vehicle dynamics and robust front wheel steering control," *IEEE Trans. Control Syst. Technol.*, vol. 6, no. 3, pp. 412–420, May 1998.

[13] B. Kwak and Y. Park, "Robust vehicle stability controller based on multiple sliding mode control," in *Proc. SAE World Congr.*, Detroit, MI, 2001, no. 26-21-0003.

[14] J. Tjonnas and T. Johansen, "Stabilization of automotive vehicles using active steering and adaptive brake control allocation," *IEEE Trans. Control Syst. Technol.*, vol. 18, no. 3, pp. 545–558, May 2010.

[15] C. Garcia, D. Prett, and M. Morari, "Model predictive control: Theory and practice–a survey," *Autom. Oxford*, vol. 25, no. 3, pp. 335–348, May 1989.

[16] A. Bemporad, M. Morari, V. Dua, and E. Pistikopoulos, "The explicit linear quadratic regulator for constrained systems," *Automatica*, vol. 38, no. 1, pp. 3–20, Jan. 2002.

[17] A. Bemporad and M. Morari, "Control of systems integrating logic, dynamics, and constraints," *Automatica*, vol. 35, no. 3, pp. 407–427, 1999.

[18] S. Di Cairano, M. Lazar, A. Bemporad, and W. Heemels, "A control Lyapunov approach to predictive control of hybrid systems," in *Hybrid Systems: Computation and Control* (Lecture Notes in Computer Science). New York: Springer-Verlag, 2008, pp. 130–143.

[19] P. Ortner and L. del Re, "Predictive control of a diesel engine air path," *IEEE Trans. Control Syst. Technol.*, vol. 15, no. 3, pp. 449–456, May 2007.

[20] G. Stewart and F. Borrelli, "A model predictive control framework for industrial turbodiesel engine control," in *Proc. 47th IEEE Conf. Decision Control*, Cancun, Mexico, Dec. 2008, pp. 5704–5711.

[21] S. Di Cairano, D. Yanakiev, A. Bemporad, I. Kolmanovsky, and D. Hrovat, "An MPC design flow for automotive control and applications to idle speed regulation," in *Proc. 47th IEEE Conf. Decision Control*, Dec. 2008, pp. 5686–5691.

[22] F. Borrelli, A. Bemporad, M. Fodor, and D. Hrovat, "An MPC/hybrid system approach to traction control," *IEEE Trans. Control Syst. Technol.*, vol. 14, no. 3, pp. 541–552, May 2006.

[23] S. Di Cairano, A. Bemporad, I. Kolmanovsky, and D. Hrovat, "Model predictive control of magnetically actuated mass spring dampers for automotive applications," *Int. J. Control*, vol. 80, no. 11, pp. 1701–1716, 2007.

[24] H. Borhan, A. Vahidi, A. M. Phillips, M. L. Kuang, I. V. Kolmanovsky, and S. Di Cairano, "MPC-based energy management of a power-split hybrid electric vehicle," *IEEE Trans. Control Syst. Technol.*, vol. 20, no. 3, pp. 593–603, May 2012.

[25] G. Ripaccioli, A. Bemporad, F. Assadian, C. Dextreit, S. Di Cairano, and I. Kolmanovsky, "Hybrid modeling, identification, and predictive control: An application to hybrid electric vehicle energy management," in *Hybrid Systems: Computation and Control* (Lecture Note in Computer Science). New York: Springer-Verlag, 2009, pp. 321–335.

[26] P. Falcone, F. Borrelli, H. Tseng, J. Asgari, and D. Hrovat, "MPC-based yaw and lateral stabilisation via active front steering and braking," *Veh. Syst. Dynamics*, vol. 46, no. 1, pp. 611–628, 2008.

[27] G. Ferrari-Trecate, F. Cuzzola, D. Mignone, and M. Morari, "Analysis of discrete-time piecewise affine and hybrid systems," *Automatica*, vol. 38, no. 12, pp. 2139–2146, Dec. 2002.

[28] T. Gillespie, *Fundamentals of Vehicle Dynamics*. Warrendale, PA: SAE, 1992.

[29] E. Velenis, P. Tsiotras, and J. Lu, "Optimality properties and driver input parameterization for trail-braking cornering," *Eur. J. Control*, vol. 14, no. 4, pp. 308–320, 2008.

[30] C. Ahn, H. Peng, and H. Tseng, "Robust nonlinear observer to estimate road friction coefficient and tire slip angle," in *Proc. 10th Int. Symp. Adv. Veh. Control*, Loughborough, U.K., 2010.

[31] H. Pacejka, *Tyre and Vehicle Dynamics*. Warrendale, PA: SAE, 2006.

[32] C. Ahn, H. Peng, and H. Tseng, "Robust estimation of road friction coefficient," in *Proc. Amer. Control Conf.*, San Francisco, CA, Jul. 2011, pp. 3948–3953.

[33] A. Bemporad, F. Borrelli, and M. Morari, "On the optimal control law for linear discrete time hybrid systems," in *Hybrid Systems: Computation and Control* (Lecture Note in Computer Science). New York: Springer-Verlag, 2002, pp. 105–119.

[34] C. Floudas, *Nonlinear and Mixed-Integer Optimization: Fundamentals and Applications*. Oxford, U.K.: Oxford Univ. Press, 1995.

[35] S. Boyd and L. Vandenberghe, *Convex Optimization*. Cambridge, U.K.: Cambridge Univ. Press, 2004.

[36] S. Di Cairano, D. Yanakiev, A. Bemporad, I. V. Kolmanovsky, and D. Hrovat, “Model predictive idle speed control: Design, analysis, and experimental evaluation,” *IEEE Trans. Control Syst. Technol.*, vol. 20, no. 1, pp. 84–97, Jan. 2012.

[37] S. Di Cairano, W. Liang, I. Kolmanovsky, M. Kuang, and A. Phillips, “Engine power smoothing energy management strategy for a series hybrid electric vehicle,” in *Proc. Amer. Control Conf.*, San Francisco, CA, Jul. 2011, pp. 2101–2106.

[38] D. Piyabongkarn, R. Rajamani, J. Grogg, and J. Lew, “Development and experimental evaluation of a slip angle estimator for vehicle stability control,” *IEEE Trans. Control Syst. Technol.*, vol. 17, no. 1, pp. 78–88, Jan. 2009.

Stefano Di Cairano (M’08) received the Laurea degree in computer engineering and the Ph.D. degree in information engineering from the University of Siena, Siena, Italy, in 2004 and 2008, respectively. He was also granted the International Curriculum Option for Doctoral Studies in Hybrid Control for Complex Distributed and Heterogeneous Embedded Systems.

He was a Visiting Student with the Technical University of Denmark, Lyngby, Denmark, from 2002 to 2003, and with the Control and Dynamical Systems Department, California Institute of Technology, Pasadena, from 2006 to 2007. From 2008 to 2011, he was first a Senior Researcher and then a Technical Expert with Powertrain Control R&A, Ford Research and Innovation, Dearborn, MI. Since 2011, he has been with the Mitsubishi Electric Research Laboratories, Mechatronics Group, Cambridge, MA. His current research interests include advanced control strategies for complex mechatronic systems in automotive, factory automation, and aerospace, model predictive control, constrained control, networked control systems, hybrid systems, and robotics.

Dr. Di Cairano has been a Chair of the IEEE CSS Technical Committee on Automotive Controls since 2011 and a member of the IEEE CSS Conference Editorial Board.

Hongtei Eric Tseng received the B.S. degree from the National Taiwan University, Taipei, Taiwan, in 1986, and the M.S. and Ph.D. degrees from the University of California, Berkeley, in 1991 and 1994, respectively, all in mechanical engineering.

He joined the Ford Motor Company in 1994, where he is currently a Technical Leader with the Research and Innovation Center. His previous work includes a low-pressure tire warning system using wheel speed sensors, traction control, electronic stability control, roll stability control, and dry clutch powershift control. His current research interests include powertrain and vehicle dynamics control.

Daniele Bernardini was born in 1982. He received the Master’s degree in computer engineering and the Ph.D. degree in information engineering from the University of Siena, Siena, Italy, in 2007 and 2011, respectively.

He was a Visitor to the Department of Electrical Engineering, Stanford University, Stanford, CA, in 2010. In 2011, he joined the Department of Mechanical and Structural Engineering, University of Trento, Trento, Italy. In October 2011, he joined the IMT Institute for Advanced Studies Lucca, Lucca, Italy, where he is currently a Post-Doctoral Research Fellow. His current research interests include model predictive control, stochastic control, networked control, and their applications to automotive, aerospace, and energy systems.

Alberto Bemporad (F’00) received the Master’s degree in electrical engineering and the Ph.D. degree in control engineering from the University of Florence, Florence, Italy, in 1993 and 1997, respectively..

He was with the Center for Robotics and Automation, Department of Systems Science and Mathematics, Washington University, St. Louis, from 1996 to 1997, as a Visiting Researcher. From 1997 to 1999, he was a Post-Doctoral Fellow with the Automatic Control Laboratory, ETH Zurich, Zurich, Switzerland, where he worked as a Senior Researcher from 2000 to 2002. From 1999 to 2009, he was with the Department of Information Engineering, University of Siena, Siena, Italy, becoming an Associate Professor in 2005. From 2010 to 2011, he was with the Department of Mechanical and Structural Engineering, University of Trento, Trento, Italy. Since 2011, he has been a Full Professor and the Deputy Director of the IMT Institute for Advanced Studies Lucca, Lucca, Italy. In 2011, he co-founded ODYS S.r.l., a spinoff company of IMT Lucca. He has published more than 230 papers in the areas of model predictive control, hybrid systems, automotive control, multiparametric optimization, computational geometry, robotics, and finance. He is the author or co-author of various MATLAB toolboxes for model predictive control design, including the Model Predictive Control Toolbox (The Mathworks, Inc.).

Prof. Bemporad was an Associate Editor of the IEEE TRANSACTIONS ON AUTOMATIC CONTROL from 2001 to 2004 and a Chair of the Technical Committee on Hybrid Systems of the IEEE Control Systems Society from 2002 to 2010.